Renewable Energy 183 (2022) 651–661

Contents lists available at ScienceDirect

Renewable Energy

journal homepage: www.elsevier.com/locate/renene

Amorphous carbon based nanofluids for direct radiative absorption in solar thermal concentrators – Experimental and computational study

Anurag Pramanik [a], Harjit Singh [a, *], Ram Chandra [b], Virendra Kumar Vijay [b], S. Suresh [c]

[a] Institute of Energy Futures, College of Engineering, Design and Physical Sciences, Brunel University London, Uxbridge UB8 3PH, United Kingdom
[b] Center for Rural Development and Technology, Indian Institute of Technology Delhi, Hauz Khas, New Delhi 110016, India
[c] Department of Mechanical Engineering, National Institute of Technology, Tiruchirappalli 620015, Tamil Nadu, India

ARTICLE INFO

Article history:
Received 6 August 2021
Received in revised form
8 November 2021
Accepted 11 November 2021
Available online 17 November 2021

Keywords:
Asymmetric compound parabolic concentrator
COMSOL Multiphysics
Optical efficiency
Ray optics
Solar thermal concentrators (STC)
Nanofluids

ABSTRACT

Directly solar radiation absorbing nanofluids have the potential to absorb a wide spectrum of solar radiation and displace selectively coated metallic receivers in solar thermal collectors. Parameters including nanoparticle concentration, synthesis and storage conditions, can influence their long-term usage. In this study, 60 min was found to be optimal sonication duration to synthesise a uniform suspension of nanofluid containing amorphous-carbon nanoparticles and ethylene glycol as base fluid. Nanoparticle concentration can be used to tune extinction coefficient of nanofluid in the range of 75 −400 m^{-1} for wavelength range of 320–1000 nm. Long-term stability and high temperature studies showed a time and temperature dependent increase in transmittance of nanofluid which is restored by 5 min of stirring. Computational modelling highlighted the role of incident intensity, nanoparticle concentration as well as inlet flow rate on receiver exit temperature. A ray-optics model employing weather data for Delhi (India) can predict the optical efficiency of an Asymmetric Compound Parabolic Concentrator solar collector. This combined approach can enable to predict the flow rate required to achieve a desired supply temperature at target locations. This rational framework combining experimental and computational approaches can be used to identify design parameters relevant for application of nanofluids in thermal collectors.

1. Introduction

The use of solar energy for electricity generation, desalination and thermal applications has significantly increased owing to advances in receiver designs to enhance optical efficiency as well as reduce heat losses and improved sun-tracking mechanisms [1]. One of the promising advances is the development of directly, volumetrically absorbing nanofluids [2–4], which can be used as working fluids in solar thermal systems equipped with glass receivers to allow solar radiation to be directly absorbed by the working fluid. In contrast, the conventional receiver designs use selectively coated metal pipes which transfer the heat to the fluid via conduction and subsequently via convection in the bulk of the fluid. The metal pipes also lead to larger convective and radiative losses, which are significantly reduced in nanofluid using glass receivers [5,6]. Nanofluids, a suspension of nanoparticles in heat transfer fluids, can significantly enhance (by up to 7 orders of magnitude) the solar energy absorption capability of working fluids and therefore, the use of nanofluids holds a huge potential in solar thermal applications [2,5,7,8].

Various parameters can influence nanofluid properties including nanoparticle type, concentration [9], sonication duration [10,11] as well as choice and amount of surfactant [12–15]. Nanofluid stability is one of the major challenges for their applications in solar energy systems [16,17]. Especially for their use with Concentrating Solar Thermal (CST) panels, nanofluids can reach very high temperatures which can influence the stability of the suspension. Hence, protocols for efficient synthesis as well as maintaining long-term and high temperature stability of nanofluids are important for widespread application of nanofluids for solar thermal applications.

Another challenge with solar energy systems is the variability in incident intensity of sunlight. Advances have been made to improve the efficiency of radiation capture with a lower footprint by using innovative mirror designs and geometries [18]. For practical applications when a desired temperature is specified a priori, several

* Corresponding author.
E-mail address: Harjit.Singh@brunel.ac.uk (H. Singh).

https://doi.org/10.1016/j.renene.2021.11.047

Nomenclature and abbreviations

Nomenclature

C_p	Specific heat capacity of the fluid (J/kg K)
e_b	Blackbody emissive power
F	View factor
G	Irradiation (W/m^2)
h	Heat transfer coefficient (W/m^2/K)
I	Incident radiation intensity (W/m^2)
J	Total radiative flux leaving a surface
k	Thermal conductivity of the fluid (W/m K)
K_e	Spectral extinction coefficient of the fluid (m^{-1})
n	Medium refractive index
P	Pressure
q	Heat flux
R	Radius of pipe (m)
S	Solar-weighted absorptivity of the fluid
T	Temperature (K)
u	Velocity vector
$\dot{V}$	Volumetric flow rate L/h
y	Depth (cm)

Abbreviations

a-C	Amorphous carbon
ACPC	Asymmetric compound parabolic concentrating
CST	Concentrating solar thermal
SDS	Sodium dodecyl sulfate
STC	Solar thermal concentrators

Greek symbols

ε	Surface emissivity of glass pipe
η	Optical efficiency
θ_i	Angles of incidence
λ	Wavelength
ρ	Density of fluid
ρ_d	Diffuse reflectivity of the surface
σ	Boltzmann constant
τ	Transmittance of the fluid

Subscript

amb	Ambient
ext	External
in	Inlet
m	Mutual surface radiation

parameters such as incident intensity, flow rate (or residence time) of fluid, ambient temperature, and fluid properties can influence the ability of solar collector to meet this demand. A framework that describes the effect of a selection of climatic and nanofluid properties on the exit temperatures is essential to optimize and predict the inlet conditions to achieve a desired exit temperature.

COMSOL Multiphysics has been successfully benchmarked and used to model various phenomena including diffusion and fluid flow [19–21], surface-to-surface radiation to model radiative heat transfer [22–25] as well as ray trajectories [18], which can enable design and compare energy efficient solutions by incorporating multiple phenomena. Various methods have been incorporated in its in-built modules which can be coupled and simultaneously solved at each time step. Therefore, the application of COMSOL based models in solar applications is very promising.

In this study, a combined experimental and computational approach to rationally design the various aspects of nanofluid for their successful and efficient incorporation with CST was developed. The synthesis conditions of nanofluids containing amorphous carbon nanoparticles in ethylene glycol were optimised for their use in solar thermal applications. Amorphous carbon based nanofluids have a broad absorption spectrum which makes them suitable for absorbing UV, visible and near infrared wavelengths is shown. Methods to tune the optical properties as well as maintain the stability of nanofluids for long duration and at high temperatures were highlighted. COMSOL Multiphysics models, were developed to a) describe the relationship of different working conditions such as inlet flow rate, incident intensity, and nanoparticle concentration on the temperature profile of receiver pipe, b) identify the optimum nanoparticle concentration for efficient solar absorption, c) estimate the incident intensity on the receiver tube (by using real-life climate data) and d) predict the flow conditions necessary to maintain a desired supply temperature in Delhi, India. The combined experimental and computational approach allows the key parameters to be determined for the CST systems for global locations.

2. Methods

2.1. Nanofluid synthesis

Amorphous carbon nanoparticles, ≤80 nm particle size (average size of 40 nm and maximum 80 nm; Catalogue number 633100), ethylene glycol (Catalogue number 324558), and Sodium Dodecyl Sulfate (Catalogue number 112533) were sourced from Sigma-Aldrich. Different concentrations of nanofluids were prepared using the two-step method whereby the different amounts of nanoparticles and 1% wt/vol anionic surfactant, Sodium Dodecyl Sulfate (SDS), were added to ethylene glycol. The amount of surfactant is consistent for ethylene glycol based nanofluids [26]. To create a uniform suspension, the mixture was sonicated using a bath-type sonicator (Part number Zeronebs1nx2y7q4) for different durations (30 min, 60 min, 90 min) at a double-frequency ultrasonication power of 28 kHz.

2.2. Transmittance measurements

The optical properties of nanofluids developed were characterized by measuring the spectral transmittance for a sample thickness of 1 cm using a UV–Vis spectrophotometer over the wavelength range of 320–1000 nm. It is also known that ethylene glycol absorbs a majority of the near infrared region in the wavelength range of 1500–2500 nm [27]. The combined 320–2500 nm constitutes to ~84% of total solar irradiance [28]. Air (empty cuvette) was used as a standard reference for all measurements. 1 ml of nanofluid or ethylene glycol was added to the cuvette for measurement. All measurements were performed at room temperature.

The effect of stirring on the optical properties of the nanofluids was studied by first sampling from an undisturbed sample and then stirring using a magnetic stirrer at 250 rpm for different durations. For studying the effect of temperature, the samples were heated on a hot plate through different fluid temperatures and then allowed to naturally cool to room temperature (~1 h) for transmittance measurement.

2.3. Calculations of extinction coefficient and solar-weighted absorptivity

To assess the nanofluid properties, the solar-weighted absorptivity of nanofluid was evaluated using the equations detailed in Bhalla et al., 2018 [9]. The solar-weighted absorptivity of the fluid is given by Eq. (1),

$$S(y) = \frac{\int_0^{\lambda} G(\lambda)\left(1 - e^{-y^* K_e(\lambda)}\right) d\lambda}{\int_0^{\lambda} G(\lambda)} \quad (1)$$

where, $S(y)$ is the solar-weighted absorptivity of the fluid.

$G(\lambda)$ is the irradiation at a given wavelength, λ
$K_e(\lambda)$ is the spectral extinction coefficient of the fluid for a given wavelength, λ
y is the depth

The spectral extinction coefficient is related to transmittance based on the Beer-Lambert law and is given by Eq. (2),

$$\tau(y, \lambda) = e^{-y^* K_e(\lambda)} \quad (2)$$

where $\tau(y, \lambda)$ is the transmittance of the fluid at a given depth, y, and wavelength, λ

Based on the transmittance measurements at a known depth of 1 cm, the extinction coefficient $K_e(\lambda)$ was evaluated for all wavelengths in the 320–1000 nm range and used to evaluate the solar-weighted absorptivity of fluids at different depths.

2.4. COMSOL based modelling of directly absorbing solar collector and nanofluid system

A COMSOL Multiphysics based model is used to study the effect of radiative absorption as well as flow conditions in a receiver pipe containing nanofluids. Standard evacuated glass tubular receiver (length 1.8 m and diameter 0.043 m) ubiquitously used in commercial solar collectors was employed for the simulation (schematic is shown in Fig. 1). The inlet and ambient temperatures were assumed to be 25 °C.

The solar radiation is assumed to be entering normally to the surface of the glass pipe (receiver pipe). This pipe is encapsulated by another pipe and the annulus region is evacuated to minimize the heat loss to the surrounding. For air, the convective heat transfer coefficient is in the range of 1–500 W/m^2/K depending on wind speeds and whether it is forced or free convection. Since the encapsulating pipe is evacuated, the heat loss from the receiver pipe is assumed to be on the lower end and the heat transfer coefficient was assumed to be, h = 1 W/m^2/K [29]. The physicothermal properties of the nanofluid (thermal conductivity, specific heat capacity, viscosity, and density) were approximated to be the same as that of the base fluid. This is consistent with experimental evidence where these properties were not significantly affected by the presence of small amounts of nanoparticles [27]. The temperature dependence of the properties was considered by using material definitions of ethylene glycol in COMSOL Multiphysics. The fluid flow model was coupled with the heat transfer module to model the temperature profile. The fluid is assumed to be Newtonian, and the physics and the boundary conditions used in this study are described in Eqs. (3)–(17).

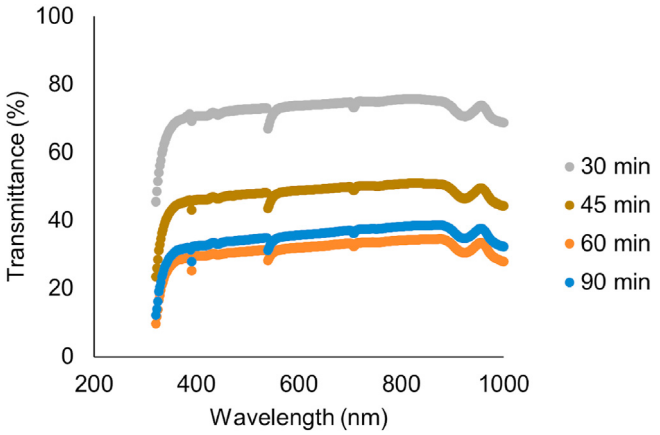

Fig. 2. Transmittance measured for different duration of sonication for nanoparticle concentration of 60 mg/L.

Laminar fluid flow was modelled using the Navier Stokes equation:

$$\rho \frac{\partial \boldsymbol{u}}{\partial t} + \rho(\boldsymbol{u}.\nabla)\boldsymbol{u} = \nabla\left[-P + \mu\left(\nabla \boldsymbol{u} + (\nabla \boldsymbol{u})^T\right)\right] \quad (3)$$

where ρ is density of fluid, $\boldsymbol{u}$ is the velocity vector, P is the pressure.

Mass conservation equation is given by,

$$\rho \nabla.\boldsymbol{u} = 0 \quad (4)$$

No slip boundary condition is used on the surface of the pipe,

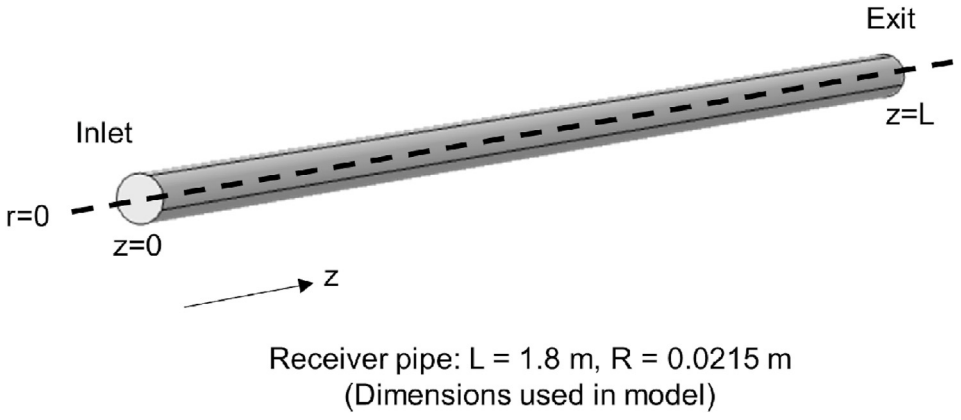

Fig. 1. Schematic of receiver pipe modelled using COMSOL Multiphysics.

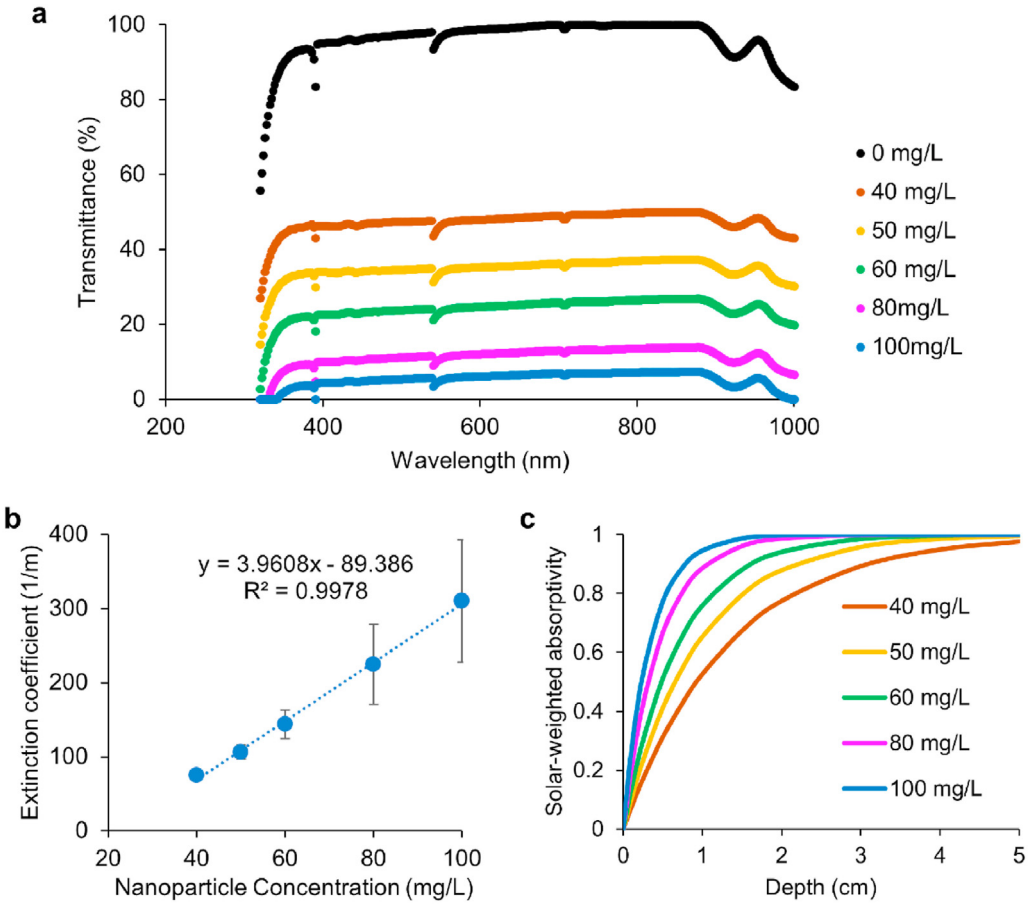

Fig. 3. a) Transmittance for nanofluids synthesized with different concentrations of a-C nanoparticles. b) The extinction coefficient for each wavelength as a function of nanoparticle concentration. c) Solar-weighted absorptivity of nanofluid as a function of depth for different nanoparticle concentrations.

given by,

$$\boldsymbol{u}|_{r=R} = 0 \tag{5}$$

where R is the radius of pipe. The inlet flow rate is specified as a boundary condition.

$$\dot{\boldsymbol{V}}|_{z=0} = V_{in} \tag{6}$$

where $\dot{\boldsymbol{V}}$ is the volumetric flow rate and V_{in} is the inlet volumetric flow rate.

The heat transfer in the fluid is modelled using the following heat equation:

$$\rho C_p \frac{\partial T}{\partial t} + \rho C_p \boldsymbol{u}.\nabla T + \nabla.\boldsymbol{q} = Q \tag{7}$$

where $C_p$is the specific heat capacity of the fluid and $\boldsymbol{q}$ is the heat flux, which is given by,

$$\boldsymbol{q} = -k\nabla T \tag{8}$$

where k is the thermal conductivity of the fluid.

The inlet temperature was fixed leading to

$$\boldsymbol{T}|_{z=0} = T_{in} \tag{9}$$

Convective heat transfer to the surroundings is modelled using the convective heat flux equation shown by Eq. (10).

$$\boldsymbol{q}|_{r=R} = h(T_{amb} - \boldsymbol{T}|_{r=R}) \tag{10}$$

where h is the heat transfer coefficient and T_{amb} is the ambient temperature.

Surface-to-surface radiation module was used to model the radiative heat loss from the receiver pipe. The equations used for modelling this are shown below:

$$J = \varepsilon e_b(T) + \rho_d G \tag{11}$$

$$G = G_{amb} + G_{ext} + G_m(J) \tag{12}$$

$$G_{amb} = F_{amb} e_b(T_{amb}) \tag{13}$$

$$e_b(T) = n^2 \sigma T^4 \tag{14}$$

where J is the total radiative flux leaving a surface, ε is surface emissivity of glass pipe, which is set to 0.9, ρ_d is diffuse reflectivity of the surface $(1-\varepsilon)$, $e_b(T)$ is the blackbody emissive power, σ is the Boltzmann constant, G is the irradiation, *amb* refers to ambient, *ext* refers to external, *m* refers to mutual surface radiation, F_{amb} is the ambient view factor and n is the medium refractive index.

The radiative absorption was modelled using Beer-Lambert Law in COMSOL Multiphysics using a similar methodology as described by Frei 2015 [30] with minor modifications due to difference in geometry. But the underlying principle remains same, i.e., the intensity is deposited as a power source for the fluid. Since it is

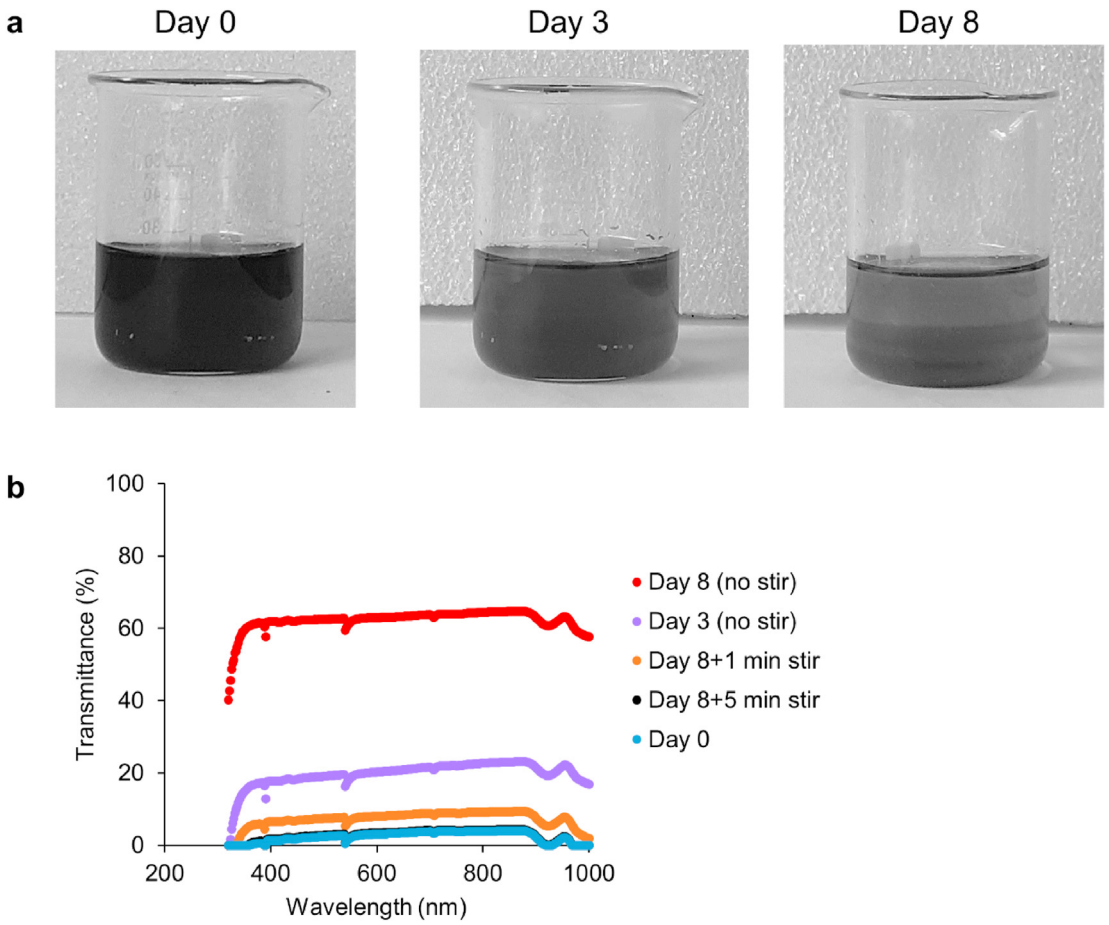

Fig. 4. a) Representative photographs of nanofluid (100 mg/L) which is incubated at room temperature for different durations b) Transmittance of nanofluids when incubated at room temperature for longer durations followed by stirring at 250 rpm for 1 min or 5 min.

assumed that the solar ray enters the receiver normal to the aperture, the Beer-Lambert law can be written as Eq. (15),

$$\frac{\partial I}{\partial r} = k_e I \tag{15}$$

It was assumed that the absorption coefficient is approximately the same as the extinction coefficient (scattering is negligible). The extinction coefficients used for nanofluids containing different concentrations of amorphous carbon nanoparticles was measured during the study as described in section 2.2 and 2.3. Dirichlet boundary condition was used to specify the incident intensity (Eq. (16)),

$$I|_{r=R} = I_{in} \tag{16}$$

Finally, a partial differential equation for temperature distribution was solved by assuming that the heat source was the same as the absorbed light:

$$\rho C_p \frac{\partial T}{\partial t} - \nabla.(k\nabla T) = Q = k_e I \tag{17}$$

2.5. Modelling of optical efficiency and prediction of flow rate

To gauge the realistic incident intensity on the solar thermal concentrator, a ray optics model and real-life solar radiation data were used in this study. An Asymmetric Compound Parabolic Concentrating (ACPC) collector with a concentration ratio of 2.3 and a length of 1.8 m was chosen. ACPC concentrators can harness significant amount of diffuse radiation (for a concentration ratio of 2.3, the concentrator can harness 43.4% of diffuse radiation) and have been shown to have a superior solar absorption and optical efficiency in partly cloudy sky conditions [31]. To evaluate the optical efficiency of the ACPC collector, an indicator of its capacity to harness beam radiation, ray optics model described previously [18] was used. Solar radiation data for Delhi was retrieved from ISHRAE [32]. The hourly angle of incidence calculations for Delhi were performed by following the steps outlined in literature [33]. Average monthly optical efficiency is calculated by first evaluating the daily proportion of intensity which is focussed on the receiver pipe (daily optical efficiency) and then averaging it over a month.

3. Results and discussion

3.1. Efficient mixing using sonication for 60 min leads to optimal optical properties

The impact of sonication on optical properties of amorphous carbon (a-C) nanoparticle based nanofluids was studied first. It was observed that a 30 or 45-min sonication was insufficient to create a uniform suspension. Both 60-min and 90-min sonication durations led to a uniform suspension indicated by a low transmittance value (Fig. 2). Importantly, increasing the sonication duration from 60 min to 90 min yielded an insignificant effect and hence, it was

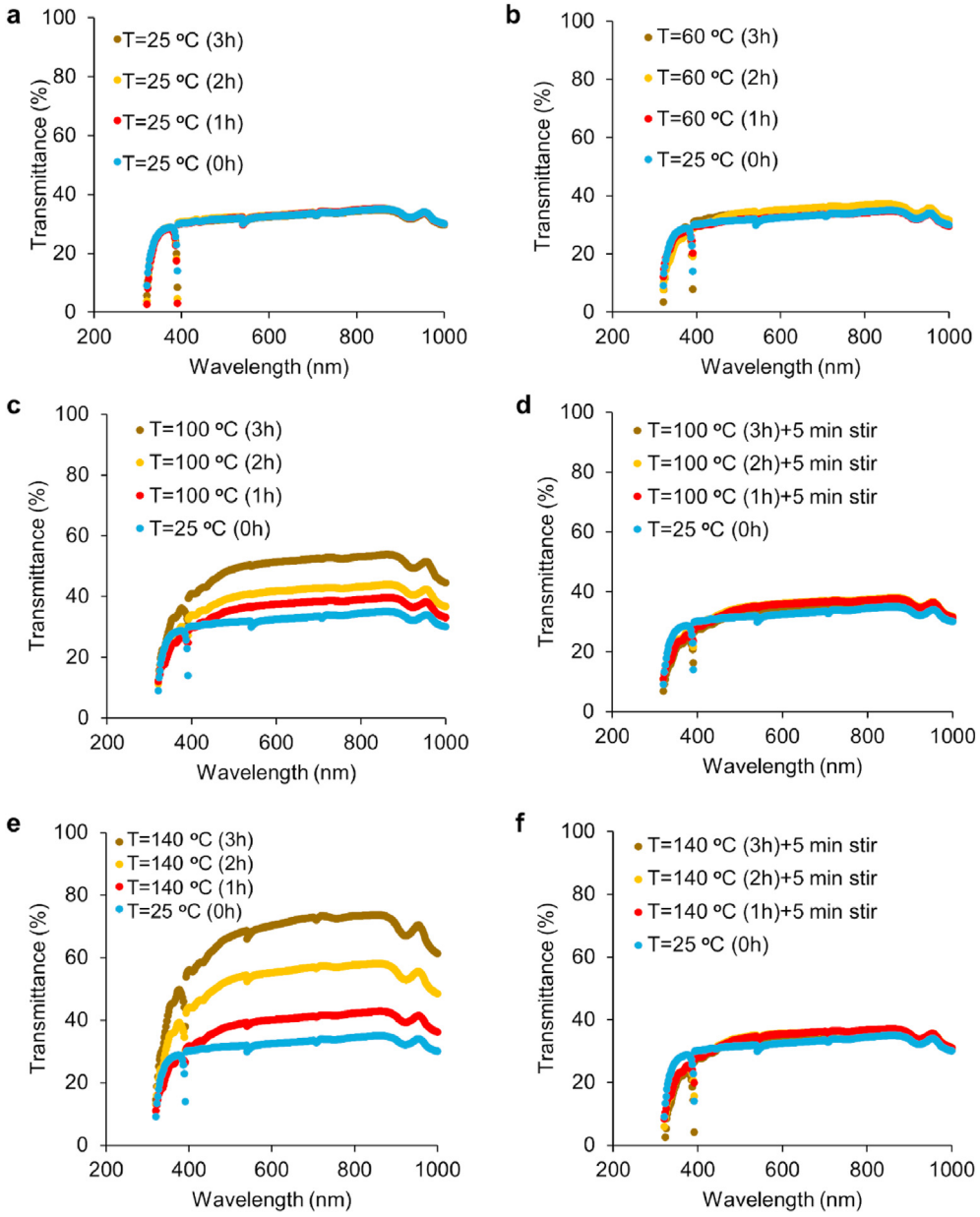

Fig. 5. Transmittance versus wavelength plot at different storage durations (1h, 2h, 3h) when the samples (60 mg/L) are left undisturbed at a) room temperature, T = 25 °C, b) T = 60 °C, c) T = 100 °C, and e) T = 140 °C. Effect of stirring for 5 min at 250 rpm prior to transmittance measurements for the samples which are heated to d) T = 100 °C and f) T = 140 °C.

concluded that a 60-min sonication duration is optimal to prepare a uniform suspension. It is important to note that these sonication studies were conducted for ethylene glycol as base fluid (viscosity: 0.0161 Pa s) using a bath sonicator with a double-frequency ultrasonication power of 28 kHz and the optimal duration is likely to vary for different base fluids or sonication frequencies.

3.2. a-C nanoparticles in ethylene glycol can absorb all wavelengths in 320–1000 nm (ultraviolet, visible and near infrared range)

Majority of solar energy is distributed in the range 320–1000 nm [28]. Therefore, the transmittance of ethylene glycol and a-C based nanofluid was measured and observed a uniform reduction in transmittance with increasing proportion of a-C for all wavelengths in this range (Fig. 3a). Importantly, the concentration of a-C nanoparticles which led to a ~5% transmittance at a depth of 1 cm (~100 mg/L) was an order of magnitude lower compared to that reported for other nanoparticles for example by Bhalla et al. [9]. The synthesized nanofluid was found to uniformly absorb the radiation wavelengths studied – an important characteristic which establishes the suitability of nanofluids for solar thermal application.

3.3. a-C nanoparticles concentration can be varied to precisely control the optical properties of nanofluid

The transmittance through the nanofluid at a depth of 1 cm was dependent on the nanoparticle concentration. The extinction coefficient for nanofluids evaluated using Eq. (2) were in the range of 75–400 m^{-1} and followed a linear relationship with the

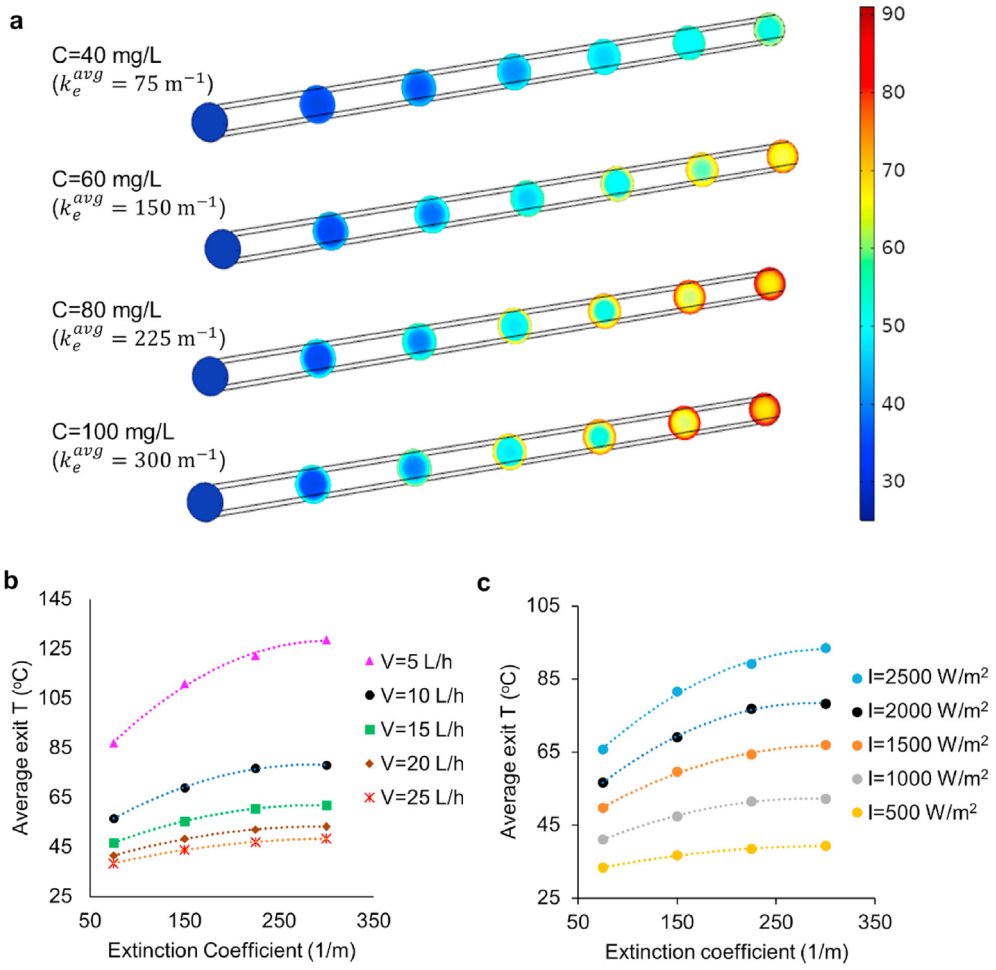

Fig. 6. a) Temperature profile for different concentrations of nanoparticle when the inlet flow rate was set to 10 L/h and incident radiative intensity 2000 W/m^2. The colour bar indicates temperature in °C. b) Average exit temperature for different extinction coefficients and inlet volumetric flow rates for an incident intensity of 2000 W/m^2. c) Average exit temperature as a function of extinction coefficient for different incident intensities (in W/m^2) at a flow rate of 10 L/h. Dotted curves in b) and c) represents a second order polynomial fit.

concentration of nanoparticles as shown in Fig. 3b. The error bars represent the standard deviation of the extinction coefficient. Finally, the extinction coefficients were employed to estimate the solar absorptivity fraction as a function of depth (shown in Fig. 3c). It was observed that concentration of nanoparticles can regulate the depth at which the solar radiation is completely absorbed. Moreover, a linear relationship of nanoparticle concentration and extinction coefficient further allows to fine-tune the optical properties of nanofluid by controlling nanoparticle concentration.

3.4. Stirring can maintain long-term stability of a-C based nanofluids

Directly absorbing nanofluid is intended for CST applications; it was important to study its long-term stability. A time-dependent settling of nanoparticles was observed as shown in Fig. 4a. An increase in the transmittance of ~15–20% when the nanofluid was stored undisturbed for 3 days was also observed (Fig. 4b). It was further found that an extended incubation of up to 8 days led to a significant settling of nanoparticles (Fig. 4b). Importantly, it was observed that stirring for 1 min at 250 rpm led to a significant restoration of nanoparticle suspension and 5 min of stirring completely restored the optical properties of nanofluid (Fig. 4b). Therefore, optical properties of a-C based nanofluids can be restored by stirring for 5 min at 250 rpm which unlocks the opportunity of developing directly absorbing nanofluid based CST plants without worrying about nanofluid performance even when plants are shut down for maintenance.

3.5. Optical properties of nanofluid are affected by high temperature

To investigate the suitability of the nanofluids for CST applications, the effects of heating on the optical properties of ethylene glycol and a-C based nanofluids were studied. At room temperature, when the nanofluid was kept undisturbed, a negligible change in transmittance after 3 h was observed (Fig. 5a). Further, maintaining the nanofluids at 60 °C for up to 3 h did not affect their stability as seen from Fig. 5b. However, when the nanofluid was heated at 100 °C, a time dependent increase in transmittance (Fig. 5c) indicating a settling of nanoparticles was observed. The transmittance values were restored with 5 min of stirring (Fig. 5d) validating our conclusion of section 3.4. Finally, heating the nanofluid to 140 °C led to a more rapid increase in transmittance (Fig. 5e). Again, it was observed that stirring for 5 min was sufficient to restore the nanofluid suspension (Fig. 5f). After 3 h of heating at 60 °C, 100 °C, and 140 °C, a temperature dependent increase in transmittance by approximately 2%, 20%, and 40%, respectively was

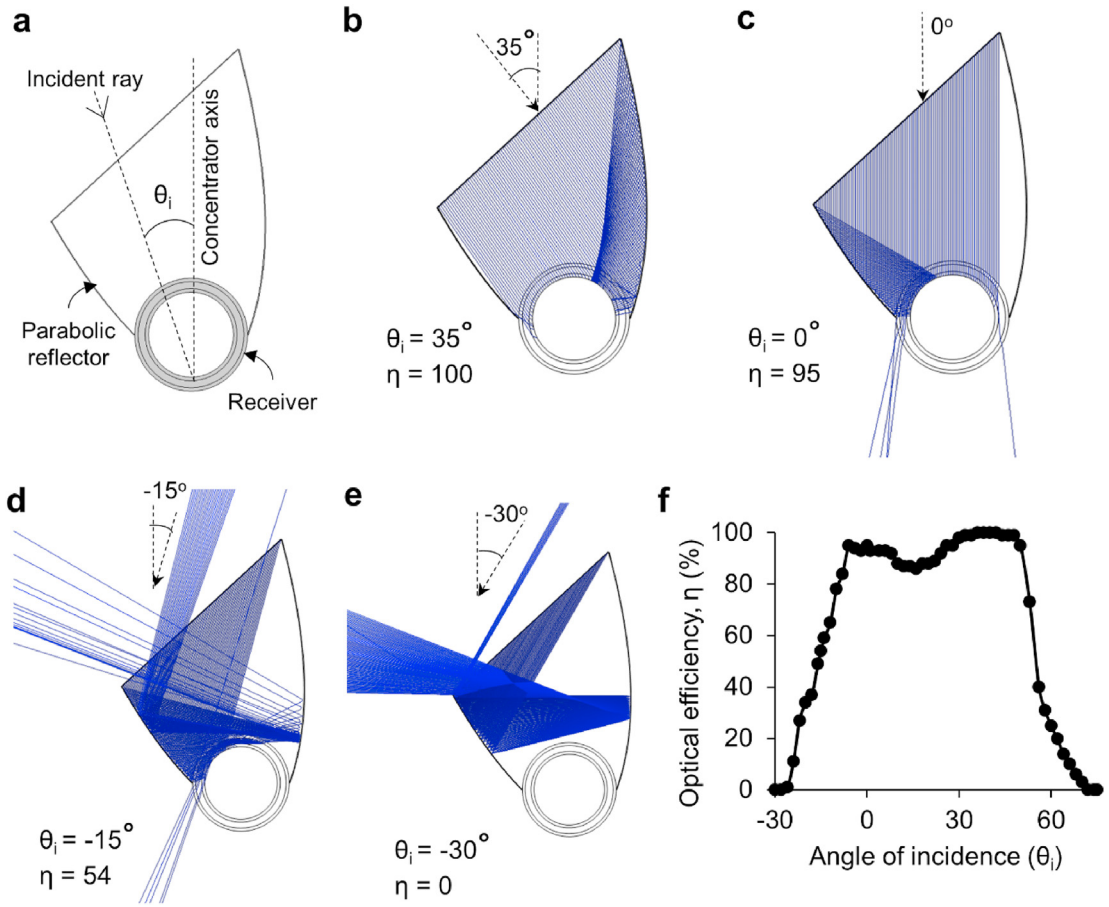

Fig. 7. a) Schematic of ACPC with concentration ratio of 2.3 modelled using COMSOL Multiphysics. The ray trajectories for an angle of incidence (θ_i)of b) 35° ($\eta = 100\%$), c) 0° ($\eta = 95\%$), d) −15° ($\eta = 54\%$), and e) −30° ($\eta = 0\%$). f) Optical efficiency (η) with varying angle of incidence (θ_i) for the modelled ACPC.

measured, when compared with those kept at room temperature (Fig. 5a, b, 5c, 5e). This behaviour is likely due to a decrease in density of ethylene glycol at higher temperatures (1129.84 kg/m^3 at 25 °C, 1077.15 kg/m^3 at 100 °C and 1049.5 kg/m^3 at 140 °C) [34] which can influence its ability to hold the nanoparticles suspended for long.

3.6. COMSOL based model of radiation absorption assuming Beer-Lambert's law highlights the significance of nanoparticle concentration in uniform heating of nanofluid

The nanofluid for solar thermal applications was modelled using COMSOL Multiphysics computational tool which assumed Beer-Lambert law for absorption of radiative flux incident on the surface of receiver. Radiative loss via surface-to-surface radiation physics and convective heat loss to the surrounding were accounted for. In direct absorption solar collectors, the nanofluid is passed through an evacuated glass pipe suffering a negligible convective loss. Finally, the heat transfer properties including specific heat capacity and thermal conductivity of nanofluid were assumed to be equal to that of the base fluid [27].

In order to efficiently use the solar radiation to uniformly heat the nanofluid flowing in a pipe, it is important to absorb solar radiation throughout the fluid. This implies that the depth at which the solar radiation must be completely absorbed must be in the range of the diameter of the pipe. A very high nanoparticle concentration can lead to complete absorption of solar radiation in a very small depth (closer to the circumference of the pipe). This will lead to very high temperatures in this region whilst the majority of the central region of the pipe receives no radiation. The heat transfer in the remaining fluid will be dominated by convection, which can be significantly slower as compared to direct radiative absorption [2]. Hence, it results in non-uniform heating of the nanofluid. This behaviour was also evident from our model (Fig. 6a). It was observed that the difference in temperature at the periphery and at the centre of the pipe increased as the nanoparticle concentration increased. On the other hand, a very low nanoparticle concentration can lead to incomplete absorption of solar radiation. Therefore, nanoparticle concentration was concluded to play a crucial role to attain uniform heating of nanofluid and maximizing solar absorption.

It was observed that increasing the nanoparticle concentration beyond a certain limit does not lead to a significant change in average temperature at the exit (Fig. 6b). Moreover, a non-linear relationship between volumetric flow rate (V) and exit temperature as increasing the flow rate from 5 L/h to 25 L/h for any extinction coefficient led a decrease in the average exit temperature which was not proportional to the change in flow rate was observed. Volumetric flow rate of nanofluid controls the residence time in the receiver pipe and hence, a lower flow rate leads to increase in average exit temperature at the cost of reduced throughput.

The role of incident radiation intensity (I) on the average exit temperature was also studied. The results for a flow rate of 10 L/h are shown in Fig. 6c. A linear relationship between intensity and average exit temperature at a selected flow rate and extinction

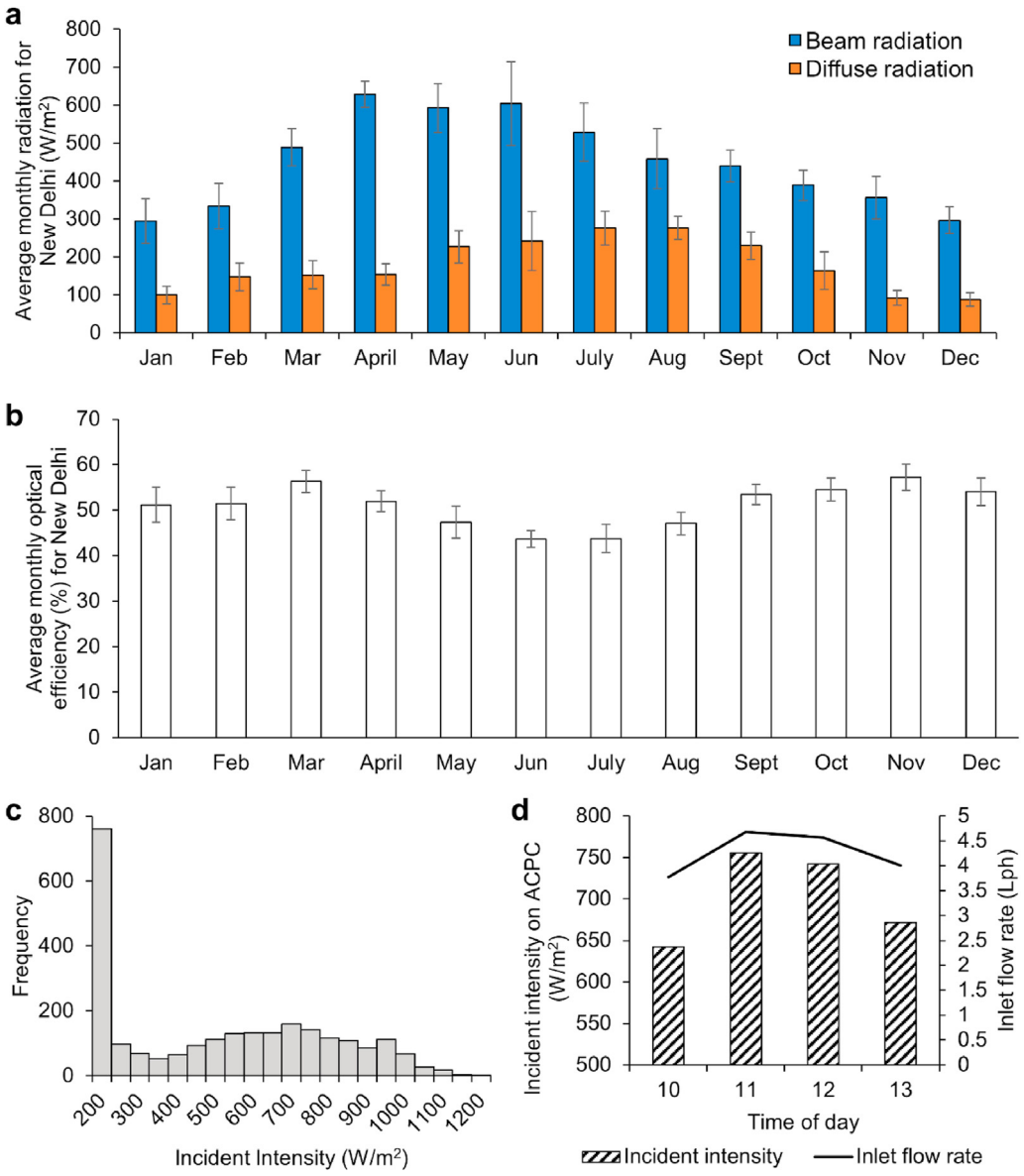

Fig. 8. a) Average monthly beam (blue) and diffuse (orange) radiation over a month for New Delhi. The error bars represent standard deviation of daily average radiation over a month. b) Average monthly optical efficiency of ACPC with a concentration ratio of 2.3 is plotted for a year. The error bars indicate standard deviation of daily optical efficiency. The detailed description of evaluation of average monthly radiation and average monthly optical efficiency is described in the methods. c) Histogram representing the distribution of incident intensity (>100 W/m^2) on the receiver pipe over a year. d) Predicted nanofluid flow rate for a day in March. The day chosen had the average ambient temperature of 25 °C in Delhi. The nanofluid was assumed to have an extinction coefficient of 150 m^{-1} (equivalent to 60 mg/L). The dimensions of the ACPC are similar to what was used in the COMSOL model (described in methods).

coefficient was observed. Therefore, using the COMSOL model developed, the concentration of nanoparticles required to deliver a known exit temperature was determined. The model also enabled to study the effects of flow rate, ambient conditions and incident intensity on average exit temperature.

3.7. Optical efficiency

An ACPC solar collector (Fig. 7a) with a geometric concentration ratio of 2.3 was simulated using ray optics module of COMSOL Multiphysics tool to estimate the optical efficiency (η) at different angles of incidence (θ_i) (Fig. 7b–e). An ACPC geometry was chosen due to its superior optical performance in locations with partly cloudy or diffuse radiation sky conditions [18,31], such as those in India during winter, autumn, and rainy seasons. A low concentration ratio of 2.3 allows up to 43.4% diffuse radiation to be concentrated enhancing the performance when it's most needed during overcast sky conditions. East-West orientation of the receiver tube with the reflectors facing True South is modelled in this simulation. The optical efficiency of greater than 90% for angles of incidence between −5° and 50° (Fig. 7f) has been predicted.

The optical efficiency of ACPC with a tilt angle of 28.5° for Delhi (Latitude 28.546 °N) was next simulated. The hourly incidence angle for a year using COMSOL model and combined this with the solar radiation data for Delhi was evaluated [32]. The distribution of average monthly beam and diffuse radiation during the 12-month period is shown in Fig. 8a. The proportion of diffuse radiation is also substantial and hence, it is important to include this in the analysis. Calculated angles of incidence and COMSOL ray optics model were employed to estimate the actual incident intensity on

the receiver tube during the day. The ratio of total daily irradiation received at the receiver tube to that reaching the aperture was calculated to estimate the daily optical efficiency which was further averaged for a month to get the monthly average optical efficiency. The distribution of monthly average optical efficiency of ACPC over a 12-month period in New Delhi is shown in Fig. 8b. For this design of ACPC, more than 50% of the daily incident irradiation in winter is focussed on the receiver. Finally, the distribution of incident intensity (>100 W/m^2) over the entire year is shown in Fig. 8c. This indicates that the maximum incident intensity was 1232.7 W/m^2 while the average during the entire year was 560.9 W/m^2.

The inlet flow rate required to achieve an average exit temperature of 60 °C on a day in March when the average ambient temperature in Delhi is 25 °C was next predicted (Fig. 8d). The COMSOL model of receiver pipe of dimensions: length = 1.8 m and radius = 0.0215 m were used. The incident intensity at different hours was calculated using both the beam as well as the diffuse component. The beam irradiation was calculated as the product of the model predicted optical efficiency and the beam irradiation for the hour and the diffuse irradiation was calculated by multiplying the diffuse acceptance factor (0.434) with the diffuse irradiation for that hour. The concentration of nanofluid was assumed to be 60 mg/L (extinction coefficient of 150 m^{-1}). Therefore, the solar irradiance data as well as ambient conditions and optical efficiency of the concentrator to identify optimum flow parameters for a given nanofluid concentration to achieve a desired temperature on the end-use side was used.

4. Conclusions

In this study, a framework which allows to design, size, and optimize the important parameters related to implementation of solar thermal collectors using nanofluids was developed. As a proof-of-concept, nanofluids, containing amorphous carbon nanoparticles and ethylene glycol, as directly absorbing solar radiation collectors for CST applications were characterized.

Nanofluids have been shown to achieve a uniform absorption in the 320–1000 nm range (UV-A, visible, and some proportion of near infrared region). The optimal sonication duration for achieving a uniform suspension of nanofluid was identified. Importantly, the optical properties of nanofluids have been shown to be tuned by modulating nanoparticle concentration. A linear relationship between the extinction coefficient and nanoparticle concentration has been observed.

The parameters which affect the stability of amorphous carbon nanoparticle based nanofluids were also studied. Incubation for longer duration as well as heating to high temperatures was found to cause settling of nanoparticles. In both cases, stirring for 5 min was sufficient to restore the optical properties of nanofluid to the same levels as freshly prepared nanofluids. Therefore, for solar thermal applications, it may be important to adopt intermittent stirring during the storage of nanofluids. This can be implemented using a stirrer in the storage tank.

To understand the impact of different nanoparticle concentrations (and hence, extinction coefficient) as well as incident intensities, a COMSOL based modelling approach to simulate heating of nanofluid flow when passing through a STC receiver whilst accounting for various heat losses including wind convective heat loss to the surrounding as well as radiative heat loss to sky was used. The effects of interfering parameters including inlet flow rate, nanoparticle concentration, and incident intensity on the average exit temperature have been studied. Our modelling approach also highlighted the relevance of choosing appropriate nanoparticle concentration for efficient heat transfer in direct absorbing collectors.

To further highlight the relevance of design of collectors, a ray optics model for an ACPC was used, to predict the optical efficiency as a function of angle of incidence. It was combined with climate data for Delhi to predict the intensity of focussed solar radiation reaching the receiver on an hourly basis. This knowledge enables to predict the flow rate as well as the collector design features to achieve a desired nanofluid exit temperature for a range of applications at global locations.

This study provides proof-of-concept for designing nanofluid based solar thermal applications using a combined experimental and computational approach which accounts for local conditions. Future studies will aim to exploit this framework to develop novel nanofluids with improved thermal and optical properties for high temperature solar thermal applications.

CRediT authorship contribution statement

Anurag Pramanik: Conceptualization, Methodology, Validation, Formal analysis, Investigation, Writing – original draft, Writing – review & editing, Visualization. **Harjit Singh:** Conceptualization, Writing – review & editing, Supervision, Project administration, Funding acquisition. **Ram Chandra:** Funding acquisition. **Virendra Kumar Vijay:** Funding acquisition. **S. Suresh:** Funding acquisition.

Declaration of competing interest

The authors declare that they have no known competing financial interests or personal relationships that could have appeared to influence the work reported in this paper.

Acknowledgements

Authors thankfully acknowledge the funding received from UK-India Education and Research Initiative (UKIERI) and Department of Science and Technology (DST), Government of India, for the COSTARMSW project through the grant agreement IND/CONT/GA/18–19/16.

References

[1] Y. Tian, C.Y. Zhao, A review of solar collectors and thermal energy storage in solar thermal applications, Appl. Energy 104 (2013) 538–553, https://doi.org/10.1016/j.apenergy.2012.11.051.
[2] V. Khullar, H. Tyagi, N. Hordy, T.P. Otanicar, Y. Hewakuruppu, P. Modi, R.A. Taylor, Harvesting solar thermal energy through nanofluid-based volumetric absorption systems, Int. J. Heat Mass Tran. 77 (2014) 377–384, https://doi.org/10.1016/j.ijheatmasstransfer.2014.05.023.
[3] T. Yousefi, F. Veysi, E. Shojaeizadeh, S. Zinadini, An experimental investigation on the effect of Al2O3–H2O nanofluid on the efficiency of flat-plate solar collectors, Renew. Energy 39 (2012) 293–298, https://doi.org/10.1016/J.RENENE.2011.08.056.
[4] S. Choudhary, A. Sachdeva, P. Kumar, Influence of stable zinc oxide nanofluid on thermal characteristics of flat plate solar collector, Renew. Energy 152 (2020) 1160–1170, https://doi.org/10.1016/J.RENENE.2020.01.142.
[5] V. Khullar, H. Tyagi, P.E. Phelan, T.P. Otanicar, H. Singh, R.A. Taylor, Solar energy harvesting using nanofluids-based concentrating solar collector, J. Nanotechnol. Eng. Med. 3 (2012), 031003, https://doi.org/10.1115/1.4007387.
[6] I.M. Mahbubul, M.M.A. Khan, N.I. Ibrahim, H.M. Ali, F.A. Al-Sulaiman, R. Saidur, Carbon nanotube nanofluid in enhancing the efficiency of evacuated tube solar collector, Renew. Energy 121 (2018) 36–44, https://doi.org/10.1016/J.RENENE.2018.01.006.
[7] N. Hordy, D. Rabilloud, J.L. Meunier, S. Coulombe, High temperature and long-term stability of carbon nanotube nanofluids for direct absorption solar thermal collectors, Sol. Energy 105 (2014) 82–90, https://doi.org/10.1016/j.solener.2014.03.013.
[8] B.A.J. Rose, H. Singh, N. Verma, S. Tassou, S. Suresh, N. Anantharaman, D. Mariotti, P. Maguire, Investigations into nanofluids as direct solar radiation collectors, Sol. Energy 147 (2017) 426–431, https://doi.org/10.1016/j.solener.2017.03.063.
[9] V. Bhalla, V. Khullar, H. Tyagi, Experimental investigation of photo-thermal

analysis of blended nanoparticles (Al2O3/Co3O4) for direct absorption solar thermal collector, Renew. Energy 123 (2018) 616–626, https://doi.org/10.1016/j.renene.2018.01.042.
[10] Y. Li, R. Kalbasi, Q. Nguyen, M. Afrand, Effects of sonication duration and nanoparticles concentration on thermal conductivity of silica-ethylene glycol nanofluid under different temperatures: an experimental study, Powder Technol. 367 (2020) 464–473, https://doi.org/10.1016/j.powtec.2020.03.058.
[11] A. Pramanik, H. Singh, S. Suresh, R. Chandra, V.K. Vijay, Identifying optimal nanofluid synthesis conditions for applications in solar thermal concentrators, in: Proc. World Renew. Energy Congr., 2021, pp. 1–6. Lisbon, Portugal.
[12] A.H.A. Al-Waeli, M.T. Chaichan, H.A. Kazem, K. Sopian, Evaluation and analysis of nanofluid and surfactant impact on photovoltaic-thermal systems, Case Stud. Therm. Eng. 13 (2019) 100392, https://doi.org/10.1016/j.csite.2019.100392.
[13] X.F. Li, D.S. Zhu, X.J. Wang, N. Wang, J.W. Gao, H. Li, Thermal conductivity enhancement dependent pH and chemical surfactant for Cu-H2O nanofluids, Thermochim. Acta 469 (2008) 98–103, https://doi.org/10.1016/j.tca.2008.01.008.
[14] H. Peng, G. Ding, H. Hu, Effect of surfactant additives on nucleate pool boiling heat transfer of refrigerant-based nanofluid, Exp. Therm. Fluid Sci. 35 (2011) 960–970, https://doi.org/10.1016/j.expthermflusci.2011.01.016.
[15] T. Aguilar, J. Navas, A. Sánchez-Coronilla, E.I. Martín, J.J. Gallardo, P. Martínez-Merino, R. Gómez-Villarejo, J.C. Piñero, R. Alcántara, C. Fernández-Lorenzo, Investigation of enhanced thermal properties in NiO-based nanofluids for concentrating solar power applications: a molecular dynamics and experimental analysis, Appl. Energy 211 (2018) 677–688, https://doi.org/10.1016/j.apenergy.2017.11.069.
[16] A. Ghadimi, R. Saidur, H.S.C. Metselaar, A review of nanofluid stability properties and characterization in stationary conditions, Int. J. Heat Mass Tran. 54 (2011) 4051–4068, https://doi.org/10.1016/j.ijheatmasstransfer.2011.04.014.
[17] K. Khanafer, K. Vafai, A review on the applications of nanofluids in solar energy field, Renew. Energy 123 (2018) 398–406, https://doi.org/10.1016/J.RENENE.2018.01.097.
[18] R.V. Parupudi, H. Singh, M. Kolokotroni, Low Concentrating Photovoltaics (LCPV) for buildings and their performance analyses, Appl. Energy 279 (2020) 115839, https://doi.org/10.1016/j.apenergy.2020.115839.
[19] A. Pramanik, S. Garg, Design of diffusion-controlled drug delivery devices for controlled release of Paclitaxel, Chem. Biol. Drug Des. 94 (2019) 1478–1487, https://doi.org/10.1111/cbdd.13524.
[20] A. Pramanik, S. Garg, Prediction of the partition coefficients using QSPR modeling and simulation of paclitaxel release from the diffusion controlled drug delivery devices, Drug Deliv. Transl. Res. 8 (2018) 1300–1312.
[21] A. Pramanik, S. Garg, Reverse engineering of diffusion-limited controlled drug delivery devices, in: Fluid Mech. Fluid Power – Contemp. Res., Springer, New Delhi, 2017, pp. 1391–1400. http://link.springer.com/10.1007/978-81-322-2743-4_133. (Accessed 23 October 2017).
[22] A.F. Emery, R.J. Cochran, H.E. Dillon, A.M. Mescher, Validation of Radiation Computations Using Viewfactors and COMSOL's Hemicube Approaches, COMSOL User Conf, 2009.
[23] S.R. Abid, N. Tayşi, M. Özakça, Three-Dimensional Thermal Modeling of Temperature VariationinConcrete Box-GirdersUsing COMSOL®, COMSOL Conf, 2014.
[24] S. Zandi, P. Saxena, N.E. Gorji, Numerical simulation of heat distribution in RGO-contacted perovskite solar cells using COMSOL, Sol. Energy 197 (2020) 105–110, https://doi.org/10.1016/j.solener.2019.12.050.
[25] P. Saxena, N.E. Gorji, COMSOL simulation of heat distribution in perovskite solar cells: coupled optical-electrical-thermal 3-D analysis, IEEE J. Photovoltaics 9 (2019) 1693–1698, https://doi.org/10.1109/JPHOTOV.2019.2940886.
[26] S.N.A. Shah, S. Shahabuddin, M.F.M. Sabri, M.F.M. Salleh, M.A. Ali, N. Hayat, N.A.C. Sidik, M. Samykano, R. Saidur, Experimental investigation on stability, thermal conductivity and rheological properties of rGO/ethylene glycol based nanofluids, Int. J. Heat Mass Tran. 150 (2020) 118981, https://doi.org/10.1016/j.ijheatmasstransfer.2019.118981.
[27] V. Khullar, V. Bhalla, H. Tyagi, Potential heat transfer fluids (Nanofluids) for direct volumetric absorption-based solar thermal systems, J. Therm. Sci. Eng. Appl. 10 (2018), 011009, https://doi.org/10.1115/1.4036795.
[28] H.D. Kambezidis, The solar resource, in: Compr. Renew. Energy, Elsevier Ltd, 2012, pp. 27–84, https://doi.org/10.1016/B978-0-08-087872-0.00302-4.
[29] P. Kosky, R. Balmer, W. Keat, G. Wise, Exploring Engineering, Academic Press, 2020, https://doi.org/10.1016/C2017-0-01871-2.
[30] W. Frei, Modeling laser-material interactions with the beer-lambert law | COMSOL blog. https://uk.comsol.com/blogs/modeling-laser-material-interactions-with-the-beer-lambert-law/, 2015.
[31] R.V. Parupudi, H. Singh, M. Kolokotroni, J. Tavares, Long term performance analysis of low concentrating photovoltaic (LCPV) systems for building retrofit, Appl. Energy 300 (2021) 117412, https://doi.org/10.1016/j.apenergy.2021.117412.
[32] ISHRAE, Weather data by Location|EnergyPlus, April 1, 2021, https://energyplus.net/weather-location/asia_wmo_region_2/IND//IND_New.Delhi.421820_ISHRAE, 2020.
[33] S.A. Kalogirou, Solar Energy Engineering, Academic Press, 2009. https://www.oreilly.com/library/view/solar-energy-engineering/9780123745019/.
[34] E. ToolBox, Ethylene glycol heat-transfer fluid, April 9, 2021, https://www.engineeringtoolbox.com/ethylene-glycol-d_146.html, 2003.